# THE ROLE OF FORGING DURING INERTIA FRICTION WELDING OF NICKEL–BASE SUPERALLOY RR1000

## K.M. OLUWASEGUN*, A.V. ADEDAYO*, A.A. ADELEKE* and O.O. OLUWOLE**

*\*\*Department of Materials Science and Engineering, Obafemi Awolowo University, Osun State, Nigeria.*

*\*\*Department of Mechanical Engineering, University of Ibadan, Oyo State, Nigeria.*

## ABSTRACT

*The dissolution response of γ' phase to thermal and mechanical effects in an inertia friction welded turbine disk nickel base superalloy RR1000 has been investigated. The thermo-mechanical affected zone (TMAZ) and heat affected zone (HAZ) microstructures around welds in a commercial PM nickel-based RR1000 superalloy were simulated using a Gleeble thermo-mechanical simulation system. Detailed microstructural examination of the simulated TMAZ and HAZ and those present in actual inertial friction welded specimens showed that γ' particles persisted during heating to the welding temperatures, where they reacted with the surrounding γ matrix producing liquid film by a eutectic-type reaction. However, it was observed that the compressive strain during the forging stage of welding significantly enhanced resistance to weld liquation cracking of the alloy by strain-assisted rapid isothermal re-solidification of the constitutional liquation products within 150μm of the bond line.*

*Keywords: Inertia friction welding; Thermo-mechanical affected zone, Heat affected zone, Nickel-based superalloys; Constitutional liquation; pre weld- cooling strain*

## 1.0    INTRODUCTION

Liquation cracking is a prominent and generic problem that is encountered during conventional welding of precipitation hardened nickel based superalloys (Thompson et al; 1998; Radhakrishnan and Thompson, 1993, Ojo et al; 2006). The development of solid state welding of unweldable nickel base superalloy is on the increase in the welding world. This is based on the premise that solid state welding takes place below the solidus of the bulk alloy. Inertia friction welding (IFW) is a welding procedure whereby one of the two work pieces is connected to a flywheel while the unconnected one is restrained from rotating. The flywheel is accelerated to a predetermined rotational speed and then disengaged from the drive, and the work-pieces are forced into contact by the application of an axial pressure. There is a themomechanically affected zone (TMAZ) inside the heat affected zone (HAZ) both having different structures from each other and different structures from the parent body. It is thus necessary to make sure these microstructures will not be deleterious to the overall performance of the material in service. A recent microstructural investigation by the present authors of an inertia friction welded turbine disc precipitation hardened nickel base

superalloy has shown that constitutional liquation of the grain boundary γ' precipitates occurred during the solid state welding in the TMAZ (Oluwasegun et al; 2010a). The extent of the liquation, and the formation of microcracks associated with liquation cracking were observed to be significantly reduced when compared with the welds of various conventional welded nickel based superalloys (Owczarski et al; 1966; Pepe and Savage, 1967; Romig et al, 1988; Reiso et al; 1993, Radhakrishnan and Thompson, 1991; Ernst et al; 1989;Ojo et al; 2004) . Infact, regions that are within 150μm from the bond line of the IFW welded alloy were observed to be liquation-crack free. It has been shown that the rapid heating of the γ' precipitates during IFW could have enhanced the precipitates to survive their solvus and thus resulted in the unexpected constitutional liquation of the precipitates within the temperature range where it is thermodynamically favourable for a γ- γ' eutectic reaction to occur Oluwasegun et al. 2010a). The on-heating formation of constitutional liquation of precipitates has been reported in various fusion welding to increase the melting range of the alloy and concomitantly lower the HAZ crack resistance of the alloy during weld cooling (Reiso et al; 1993; Ernst et al; '?9; Ojo et al, 2004). Thus, the elimination of the constitutional liquid prior to weld cooling via rapid isothermal solidification of the liquid will play an important role in improving HAZ liquation-crack resistance in welds.

In the present work, the effect of induced strain within 150μm from the bond line during the forging stage of an inertia friction welded nickel base superalloy is presented and discussed.

## 2.0    EXPERIMENTAL PROCEDURE

A new generation nickel base superalloy (RR1000) (Oluwasegun et al, 2010a; Oluwasegun et al, 2010b) designed for use as turbine disc for aero-engine has been used in this study. The standard chemical composition (wt%) of the base alloy, which has been solution heat treated at 1120°C for 4hours and aged at 760°C for 8 hours with subsequent air is shown in Table 1. The as-received inertial friction welded samples were sliced to dimensions 20mm X 12mm X 10mm. The solid state dissolution behaviour of γ' within the inertia friction welds was studied exclusively under thermal environment and under thermal environment with imposed compressive strain, both within a Gleeble thermo-mechanical simulation system. For the exclusively thermal environment, cylindrical specimens of 8mm diameter and 7.96mm length were prepared from the base alloy, heated to 1150, 1175, 1200 and 1225°C temperature at a rate of 20°C/s and held for 3s at all temperatures followed by water quenching (Figure 1a). Under thermal plus imposed compressive strain condition, samples were heated to 1225°C, held for 1sec, then subjected to 10% compressive strain in 2seconds followed by air cooling (Figure1b). Some other sets of samples were subjected to 25% compressive strain. The choice of our thermal simulation peak temperatures was based on the results of finite element simulation of the peak temperature reached during a solid state welding (inertia friction welding, IFW) as reported by Wang et al. (2005). The specimen temperature was controlled with a chromel-alumel thermocouple spot welded to the specimens at the midsection of the gauge length. The specimens under exclusively thermal environment were water quenched subsequent to the rapid heating in order to preserve, as much as possible, the microstructural changes that occurred at the simulation temperatures. The as-received inertial friction welded samples were sectioned transversely to the weld, and the Gleeble simulated samples were sectioned at the location of the spot welded

thermocouple. The sectioned samples were polished using standard metallographic techniques and were subsequently electrolytically etched in 10% orthophosphoric acid solution at 3.5 V for 3s. TEM samples were prepared by twin jet electro polishing. Due to the eroding effect of electropolishing technique on some special features of interest, a Quanta 3D FEGSEM FIB equipped with gallium focussed ion beam was used to prepare TEM samples from those specific regions of the HAZ. Phase examination and characterisation were carried out on optical microscopes, an FEI-XL30 environmental FEGSEM equipped with energy dispersive X-ray spectrometer and Tecnai F20 and Jeol 2100 Transmission Electron Microscopes (TEM), both equipped with Oxford energy dispersive X-ray spectrometry. Thermal analyses of 3mm x 1mm disc samples were performed on a Neztsch DSC 404.

showed precipitation of ~48 vol.% ordered intermetallic phase within the grain and at the grain boundaries of the $\gamma$ matrix (Figures. 2 and 3). They consisted of a fairly regular distribution of primary cuboidal $\gamma'$, 0.8–2$\mu$m in size, fine (100-500nm) spheroidal secondary $\gamma'$ and very fine tertiary $\gamma'$ (5-30nm) (Figure 2a-d). TEM selected area diffraction patterns (SADPs) from primary $\gamma'$ at three different zone axes show the precipitates to have an ordered $L1_2$ structure with lattice parameter a=3.55Å (Figure 4). Super lattice reflections from a composite SADPs from a region of both $\gamma'$ and $\gamma$ at different zone axes confirmed $\gamma'$ to be coherent with the disordered fcc $\gamma$ matrix (a=3.59Å) with a cube-cube orientation relationship (Figure 5). Other precipitates of smaller volume fractions, like Ti, Ta rich MC type carbide, Cr, Mo rich $M_3B_2$ type boride and Hf rich oxides were also observed in the solution heat treated alloy.

Table 1. Chemical composition of the base alloy.

| Element | Al | Ti | Co | Cr | Mo | Ti | Zr | Hf | C | B |
|---|---|---|---|---|---|---|---|---|---|---|
| Weight % | 3.0 | 3.9 | 16.5 | 15.0 | 5.0 | 3.9 | 0.05 | 0.2 | 0.02 | 0.02 |



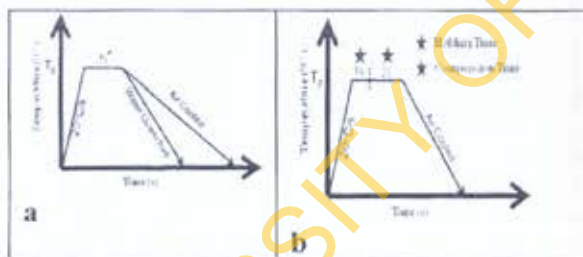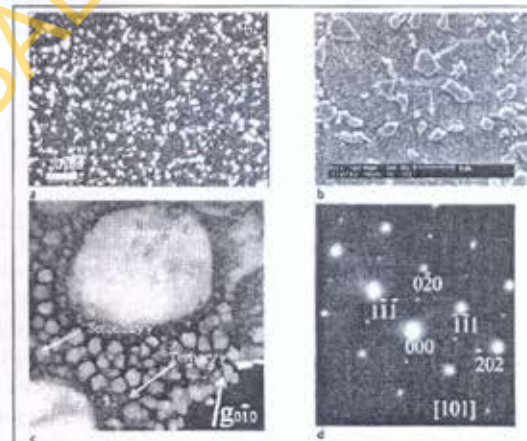*Figure 1(a) Schematic thermal profile for the exclusively simulated thermal environment (b)Schematic simulated thermal+mechanical profile.*



*Figure 2 (a) Optical micrograph showing the distribution of primary $\gamma'$ in $\gamma$ matrix (b) SEM micrograph showing primary and secondary $\gamma'$ precipitates in parent RR1000 alloy (c) TEM DF image showing primary, secondary and tertiary $\gamma'$ (d) Selected area diffraction pattern (SADP) used for the image in 'c'.*

# 3.0 RESULTS AND DISCUSSION
## 3.1. Microstructure of the base alloy.

The quantification of the $\gamma'$ precipitates in the pre-weld solution heat treated PM RR1000 superalloy using optical, scanning and transmission electron microscopy in conjunction with image J analysing software

## 3.2. Microstructures of the as-welded HAZss

Microstructural changes that occur between the weld bond line (BL) and the region where there is no detectable change in the microstructure of

the base alloy resulting from the heat and mechanical strain of inertia welding of the superalloy have been closely and carefully studied in this work. Figure.6 shows the microstructural evolution between the BL and the base material. This figure shows regions where both primary and secondary γ' are depleted (Figure 6a), region with eutectic-like features that could have resulted from localised melting of primary γ' precipitates (Figure 6b), region of incomplete liquation of the transgranular primary γ' (Figure 6c), region illustrating gradual dissolution of secondary γ' (Figures 6d-h), and region where there is no detectable change in microstructure (Parent material) (Figure 6i). These variations in the microstructures suggest thermal gradient across the weld region. The dissolution behaviour of the main strengthening phase γ' as observed between 150μm-300μm away from the bond line has been extensively discussed by the present author (Oluwasegun et al, 2010a; Oluwasegun et al, 2010b). Thus the dissolution response within 150μm of the bond line has been closely investigated and presented in the following sections.
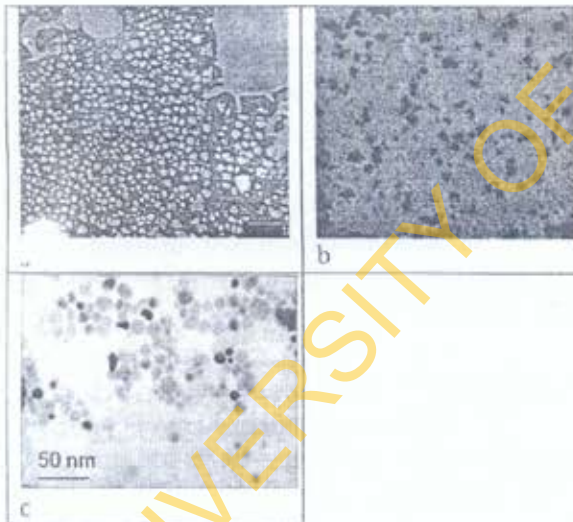


*Figure 3 (a&b) SEM BSE images of primary and secondary γ' respectively (c) Tertiary γ' extracted by carbon replica.*

### 3.3. Microstructure under exclusively thermal environment

In order to understand the dissolution behavior of γ' precipitates within the HAZ during the solid state welding, the microstructures of the HAZ were simulated exclusively under thermal environment by rapid heating of cylindrical specimens to a pre-determined temperature, using Gleeble thermo-mechanical system. The simulated HAZ microstructure of a sample rapidly
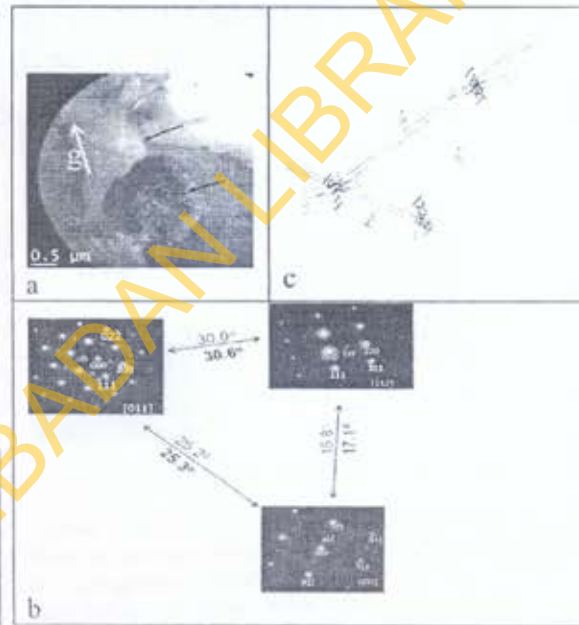


*Figure 4 (a) TEM BF image of an intergranular primary γ' particle (blue arrow shows the grain boundary and black arrow shows the primary γ'. (b) SADPs from the primary γ' in 'a' for three different zone axes. The bold angles are the measured total tilt angle while the unbold are the calculated angles. (c) A schematic Kikuchi pattern along the three zone axes in 'b'*

heated to 1150°C and water quenched showed that the intragranular secondary γ' precipitates dissolved completely and re-precipitated as very fine γ' while the primary γ' particles appeared not to be affected (Figure 7). However, in samples heated to 1175°C, primary γ' particles appeared to have survived their solvus temperature range of approximately 1148°C-1158°C, but

constitutionally liquated (Figure 8) with re-solidification features observed at the $\gamma$-$\gamma'$ interface. The solvus of $\gamma'$ precipitates were predicted from DSC and Thermo Calc. Results (Figure 9).

On increasing the simulation temperature to 1200°C complete liquation of the intergranular $\gamma'$ particles were observed (Figure 10). The microstructure of a specimen heated to 1225°C shows extensive and complete liquation of primary $\gamma'$ particles similar to what was observed at 1200°C (Figure 11). It is noteworthy to mention here that the observed constitutional liquation products in the HAZ simulated samples are very similar to what was observed between 150$\mu$m and 350$\mu$m away from the bond line of the as-welded sample as shown in figure 6.heated to 1150°C and water quenched showed that the intragranular secondary $\gamma'$ precipitates dissolved completely and re- precipitated as very fine $\gamma'$ while the primary $\gamma'$ particles appeared not to be affected (Figure 7). However, in samples heated to 1175°C primary $\gamma'$ particles appeared to have survived their solvus temperature range of approximately 1148°C-1158°C, but constitutionally liquated (Figure 8) with re-solidification features observed at the $\gamma$-$\gamma'$ interface. The solvus of $\gamma'$ precipitates were predicted from DSC and Thermo Calc. Results (Figure 9).

On increasing the simulation temperature to 1200°C complete liquation of the intergranular $\gamma'$ particles were observed (Figure 10). The microstructure of a specimen heated to 1225°C shows extensive and complete liquation of primary $\gamma'$ particles similar to what was observed at 1200°C (Figure 11). It is noteworthy to mention here that the observed constitutional liquation products in the HAZ simulated samples are very similar to what was observed between 150$\mu$m and 350$\mu$m away from the bond line of the as-welded sample as shown in figure 6.

This dissolution behaviour confirms the report of Pepe and Savage (1967) that precipitates within an austenitic matrix could survive their solvus temperature depending on the size of the precipitate and heating rate involved.
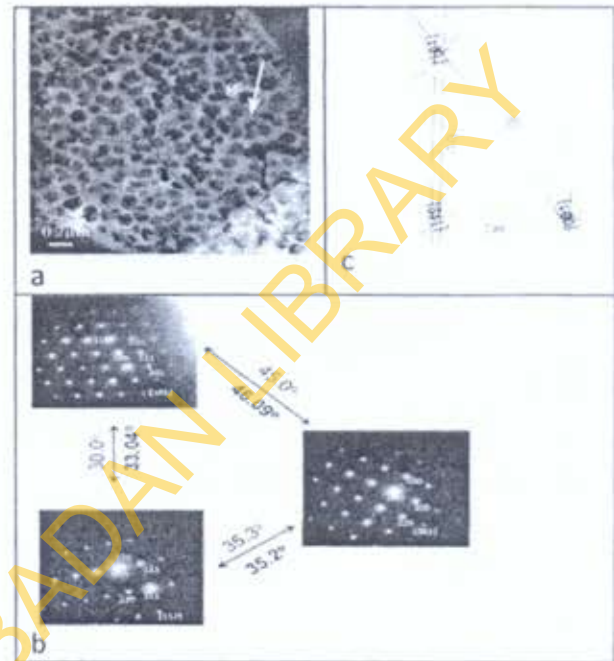


*Figure 5 (a) TEM BF image along [001] zone axis showing intragranular $\gamma'$ precipitate within the $\gamma$ matrix (b) Composite SADPs from both $\gamma$ and $\gamma'$, showing superlative reflections from the ordered $\gamma'$ coherent with the disordered $\gamma$ matrix with a cube-cube orientation relationship. The bold angles are the measured total tilt angle while the unbold are the calculated angles. (c) A schematic Kikuchi pattern along the three zone axes in 'b'.*

To further validate this proposed dissolution behaviour during rapid heating, the dissolution behaviour of the $\gamma'$ particles at equilibrium (slow heating rate) was also investigated. It was observed that the primary $\gamma'$ particles that constitutionally liquated during high heating rate (non-equilibrium), at temperatures above their solvus, dissolved without liquation in the matrix under equilibrium conditions of 5°C/min heating rate and holding time of 1hr at each temperature with subsequent air cooling. This results in the production of $\gamma$ matrix with rapidly re-precipitated very fine $\gamma'$ precipitates after cooling. The

33

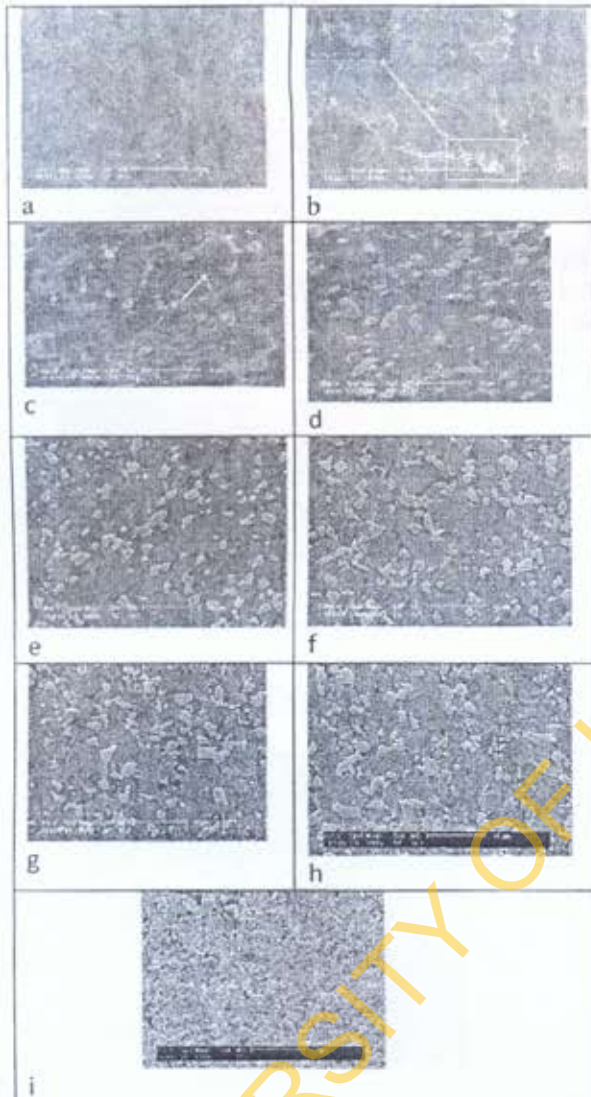micrographs showing this equilibrium dissolution are presented in figure 12.



*Figure 7: Simulated HAZ microstructure in a sample heated to 1150°C for 1s and water quenched*



*Figure 8: SEM micrograph of Gleeble sample heated to 1175°C for 1s and water quenched ;inset micrograph showing the typical crown- like morphology of re-solidified γ-γ' eutectic*



*Figure 9: (I) Thermo Calc. profile for nominal composition of RR1000 superalloy, showing phase fractions of various phases at different temperatures.*



*Figure 6 SEM images showing microstructural evolution from (a) BLZ (b) HAZ where complete primary γ' liquation occurs (c) HAZ where incomplete liquation of transgranular primary γ' occurs (d) HAZ where complete dissolution of secondary γ' occurs without liquation of primary γ' (e-h) HAZ showing gradual dissolution of secondary γ' (i) the parent material where no microstructural changes occur.*
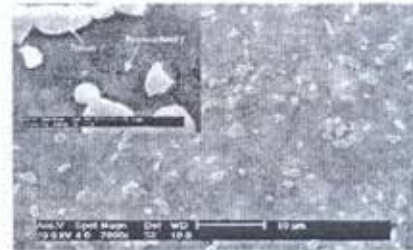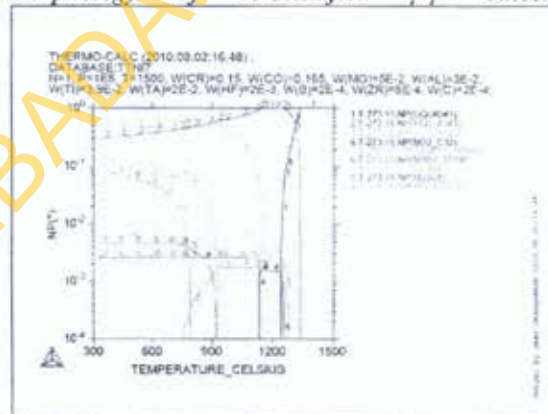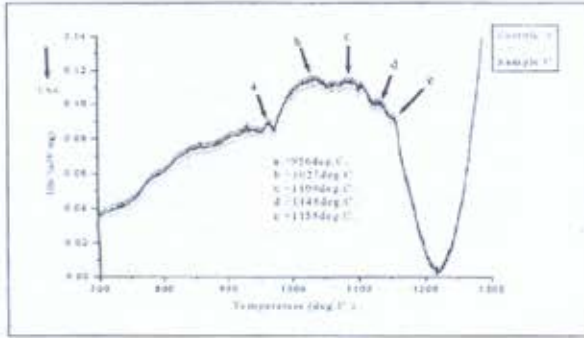
*Figure 9: (II)DSC thermal profile of γ' phase transformation in RR1000.(b-c) represent solvus temperature range of secondary γ', (d-e) represent solvus temperature range of primary γ'.*



*Figure 11: Simulated HAZ microstructure in a sample heated to 1225°C for 1s and water quenched.*

## 3.2. Microstructures under thermal and mechanical environment.

The effect of the compressive mechanical stress/strain (forging stage of weld) on the dissolution behavior of γ' precipitates during rapid heating cycle of inertia friction welding has been simulated and the microstructures carefully studied. The evolved microstructures have been compared with the microstructures of the as-welded samples.
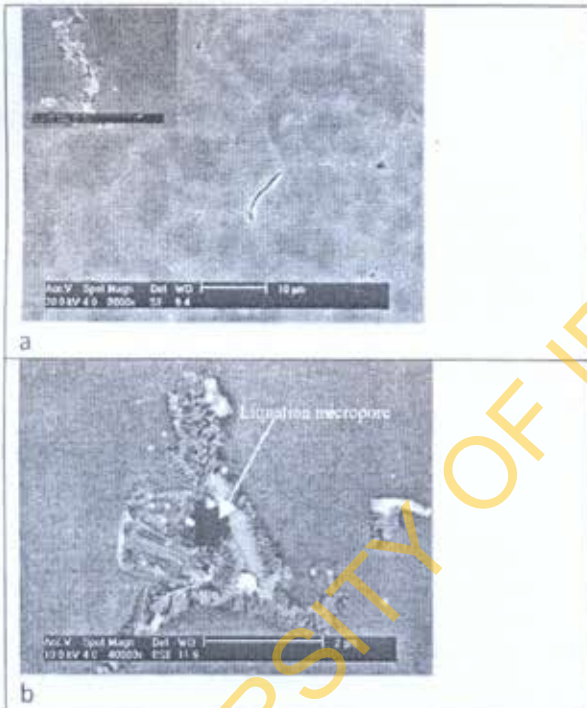


*Figure 10 (a): Simulated HAZ microstructure in a sample heated to 1200°C for 1s and water quenched, showing constitutional liquated γ' along grain boundaries (b) BSE mode micrograph showing micropores around the liquated particles.*
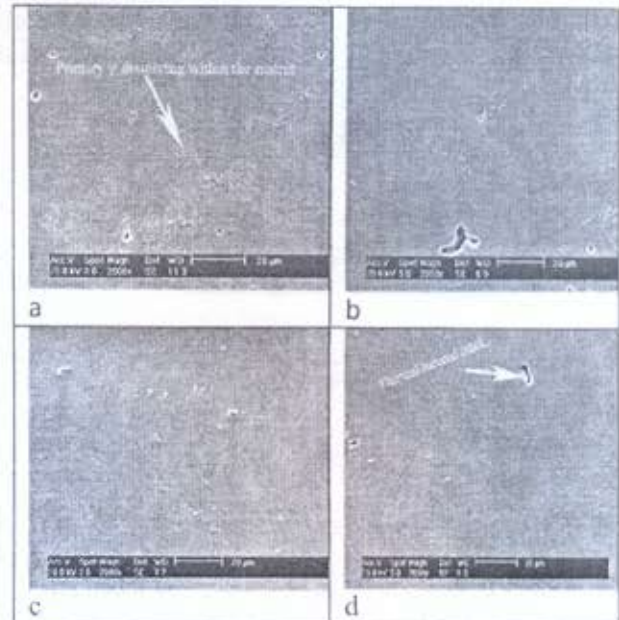


*Figure 12 SEM micrographs(x2000) of γ' dissolution under equilibrium condition at various temperatures (a) 1150°C (b) 11755°C (c) 1200°C (d) 1225°C*

Gleeble compression samples were rapidly heated to 1225°C at 20°C/s, held for 1s and strained in compression for 2 seconds at a rate of 0.05/s and 0.125/s to total strain of 10% and 25% respectively, followed by air cooling. Figures 13 and 14 show the microstructures evolution within the strained samples at the total 10% strain and 25% strain respectively. Figure 13 is characterised with few remaining eutectic product ahead of a differentially etched region. This differentially etched region has been reported in various works on liquation to be caused by the migration of liquid film (Radhakrishnan and Thompson, 1990; Barker and Purdy,1998; Nakkalil et al, 1993). Figure 14 shows complete depletion of the constitutional liquation product after applied 25% strain, which is very similar to what we observed within 150μm of the bond line of the as-welded sample (fig.6a). The proposed mechanism depicting this microstructural response within this region in the as-weld samples and the strained gleeble samples is discussed below.

### 3.3 Strain assisted rapid isothermal solidification of constitutional liquid.

With reference to the temperature prediction of the bond line region during inertia friction welding of RR1000 superalloy (Wang et al, 2005), it was expected that the microstructure of this region should be very similar to the microstructure of the Gleeble samples with peak temperatures in the range of the thermal prediction. However, our observation shows otherwise in that the re-solidified eutectic products from the constitutional liquated precipitates were not present in the TMAZ of the weld (within150μm of weld joint), but were found in the Gleeble samples exclusively under thermal condition and also in the HAZ (within 150μm-350μm away from the bond line) of the as-welded samples. This discrepancy could not be exclusively

explained via the peak temperature attained during the welding, since similar predicted temperature was employed in the Gleeble simulation. This suggests that the liquid formed within the TMAZ during the welding process could have undergone rapid isothermal solidification via another mechanism at the welding peak temperature prior to weld cooling.

Even though the effect of strain on diffusion is often unduly neglected, it has been shown that imposed strain on solids can thermodynamically drive a non-equilibrium system towards equilibrium (Embury et al. 2003). Fundamentally, the kinetics of thermodynamically driven phase transformations in materials involves atomic diffusion, which can be affected by both the magnitude and sign of externally imposed strain (Ola et al; 2010; Cowern et al, 1994). In their analytical study of vacancy assisted atomic diffusion, Cowern et al(1994) recently developed a relationship between activation energy per unit strain, Q, and diffusion coefficients under strain, D(strained), and without strain, D(relaxed), as shown in equation 1

$$D(strained) = D(relaxed) \exp\left(\frac{-Qs}{kT}\right) \quad (1)$$

where s is the strain (negative for compression and positive for tension), k is a constant and T is the absolute temperature. The equation implies a linear dependence of the activation energy of diffusion on strain. It is obvious from equation 1 that atomic diffusion can be enhanced by compressive strain and reduced by tensile strain.

With the application of this concept, Shahriari et al; (2009) and Ola et al; (2010) have been able to illustrate the dissolution of γ', which is typically known to be controlled by diffusion of γ' forming elements away from the precipitate/matrix interface to be significantly enhanced by

compressive stress in nickel base superalloys. This suggests that strain enhanced diffusion is indeed dynamic in this class of materials.

In the same vein it has been reported (Barker and Purdy, 1998) that non-equilibrium intergranular and intragranular liquid can isothermally re-solidify through solid-state back diffusion of solutes away from the liquid phase.

Rapid isothermal re-solidification of metastable liquid prior to cooling at high temperature has been reported in literatures to occur in fusion welds of various alloy systems due to (i) back diffusion of solute atoms from the liquid phase (Cowern et al; 1994; Barker and Purdy, 1998 and Ola et al; 2010), and (ii) liquid film migration (LFM) (Barker and Purdy, 1998 and Ojo et al; 2004). These two phenomena have been illustrated to be diffusion enhanced of which the amount of strain in the system is a pertinent factor as illustrated by equation 1. With reference to this equation, the higher the compressive strain, the higher the diffusivity. This therefore suggests that the induced compressive strain during the forging stage of inertia friction welding of the alloy could have significantly contributed to increased diffusion of solute atoms away from the non-equilibrium liquid phase, and thus driving the non-equilibrium system to equilibrium. This could have enhanced rapid isothermal solidification of the liquid within the TMAZ of the weld prior to cooling as reported in other alloy sytems (Cowern et al; 1994; Barker and Purdy, 1998; Embury et al; 2003 and Ola et al; 2010). It is imperative to mention here as stated earlier that re-solidified eutectic products were only observed within the HAZ of the weld which is about $150\mu m$ - $350\mu m$ away from the bond line (Figure 5b-c), which suggests that the induced strain level in this zone may be marginal or not sufficient to enhance efficient solute back

diffusion within the liquid phase. Moreover, Barker and Purdy (1998) have been able to show in their analytical model of the initial migration velocity required for a metastable liquid to rapidly solidify prior to cooling as illustrated in equation 2.

$$v = \frac{D_L\,(\Delta C)}{(C_{L,T} - C_{S,T})\delta} \qquad (2)$$

where $D_L$ is the solute diffusivity in the liquid phase, $\Delta C$ is the concentration difference across the liquid film at the start of the migration process, $C_{L,T}$ and $C_{S,T}$ are the equilibrium solute concentrations in the liquid and solid phases respectively, at the solidifying interface.

Fast intergranular liquid film solidification by LFM process has been reported to be dependent and controlled by rapid solute diffusional transport within the system (Barker and Purdy, 1998 and and Ola et al; 2010). The liquid state diffusion is primarily driven by solute concentration gradient, $\Delta C$ in the liquid, which is enhanced by the difference in composition of the liquid in contact with the two adjacent strained grains. Barker and Purdy (1998) explained that the difference in the liquid composition arises primarily by the existence of differential strain, $\Delta\varepsilon$, between the adjacent grains, which leads to the liquid composition at equilibrium with the strained solids to differ. In accordance with the diffusional coherency strain theory, generation of similar levels of coherency stress in adjacent grains is expected owing to symmetrical lattice back-diffusion, however $\Delta\varepsilon$ does exist (Handwerker et al. 1985). This has been attributed to the difference in the value of crystallographic orientation-dependent modulus of elasticity, Y, in the two grains (Handwerker et al; 1985). Thus an increase in $\Delta\varepsilon$ will produce a corresponding increase in $\Delta C$, which would imply a higher driving force for LFM. This suggests that any factor that effectively

increases the magnitude of $\Delta\varepsilon$ can accelerate the LFM process significantly (Ola et al; 2010). Thus an externally imposed compressive stress, which will generally be several orders of magnitude higher than $\Delta\varepsilon$ is involved during IFW in addition to $\Delta\varepsilon$. Ola et al. (2010) have shown that the presence of relatively large $\Delta\varepsilon$, due to the contribution from externally applied compressive stress, could significantly alter the free energy curves of the adjacent grains with respect to that of the liquid phase in between them, to enhance a relatively high $\Delta C$ value as illustrated in Figure 16. This will concomitantly result in higher migrating velocity of the liquid film and larger migrated region than to a scenario exclusively under thermal environment.

It is obvious from figures 13 and 15 that liquid film migration (differentially etched region) exists in the microstructures simulated under compressive strain and no migration region in the one without externally applied compressive strain. The LFM in figure 13 is characterized by a small amount of the dendritic eutectic feature left ahead of the differentially etched zone. Although the LFM in the 10% compressive strained Gleeble sample could not preclude liquation micropores like as observed in the microstructure within the TMAZ of the as-welded material, still it illustrates a significant migration of the liquid film under externally induced compressive strain, and thus supports the theories proposed by Cowern et al(1994) and Barker and Purdy (1998). In figure 14, the eutectic products were absent in the sample subjected to 25% compressive strain at 1225°C, which suggests isothermal re-solidification of the liquid due to strain-assisted solute back diffusion prior to cooling, because the eutectic features were present in the Gleeble sample heated to the same temperature but exclusively under thermal condition. This observed microstructure in figure 14 is very similar to the observed microstructures within the TMAZ of the as-welded alloy, which suggests that the compressive strain during the forging stage of the inertia friction welding could have aided the rapid isothermal solidification of the liquation product.

Resistance to liquation cracking via LFM has also been observed in various fusion welded nickel alloys based on other rapid solidification criteria (Radhakrishnan and Thompson, 1990; Nakkalil et al. 1993 and Barker and Purdy, 1998), but the migration extent of the liquid film is relatively smaller than what has been observed in inertia friction welding, and thus the production of crack free weld is limited in fusion welding.

It can be suggested at this point that the absence of constitutional liquation product within the TMAZ of IFW of this superalloy is not that constitutional liquation does not occur within the zone, but could have been due to sufficient amount of strain developed during the forging stage of the welding process, which could have enhanced very rapid isothermal solidification of the liquid without leaving a trace of the liquation product within this zone of the weld prior to weld cooling.
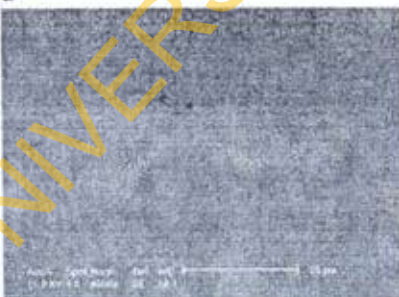
b



c

*Figure 13: SEM micrographs showing the extent of (a) liquid film migration at low magnification in thermally simulated microstructure with applied 10% external compressive strain, (b&c) higher magnification of some marked regions from 'a' intergranular liquid film migration.*

It is important to mention also that aside the proposed strain effect on rapid isothermal solidification of non-equilibrium liquid film prior to weld cooling; it may be possible for some of the liquid film formed during inertia friction welding to escape from the weld interface during the flash formation of the welding process.



a



b

*Figure 14 (a&b): Secondary electron micrographs showing the absence of eutectic products in Gleeble thermally simulated microstructure at 1225°C with applied 25% compressive strain.*
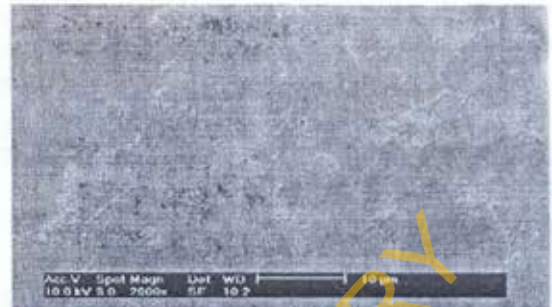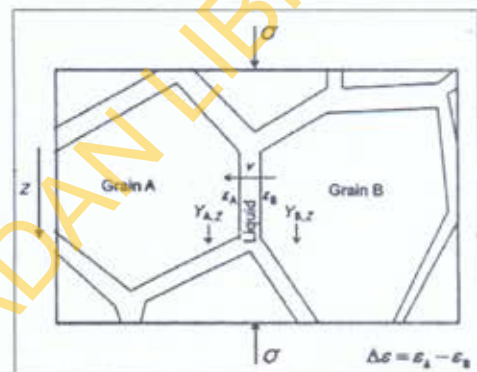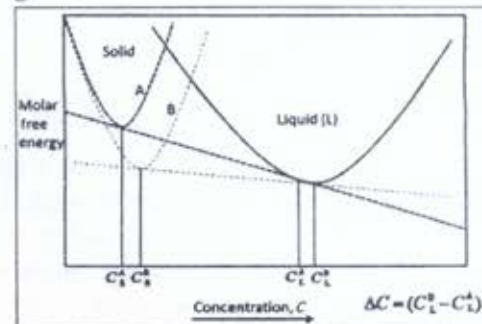


*Figure 15: SEM micrograph showing the absence of liquid film migration in thermally simulated microstructure at 1225°C without applied external compressive strain.*



a



b

*Figure 16: Shematic diagram showing (a) liquid film between two grains of different orientation-dependent elastic modulus, Y, and (b) the corresponding free energy curve. [18]*

## 4.0    CONCLUSSION

Despite the general belief that inertia friction welding is a solid state welding technique, based on the premise that the joining occurs below the equivalent melting temperature of bulk material, it has been

observed that constitutional liquation of $\gamma'$ precipitates occur within the weld of the studied superalloy during the solid state welding. However, the effectiveness of inertia friction welding in producing liquation crack-free within 150$\mu$m of the welds as compared to other conventional welding techniques has been shown to be related to the effect of induced compressive strain during the forging stage of welding on the rapid isothermal re-solidification of the constitutional liquation products within the TMAZ.

## 5.0 REFERENCES

Barker, S.W. and G.R. Purdy, (1998). "*On liquid film migration in aluminium-copper alloys*". Acta Materialia. 46(2): p. 511-524.

Cowern, N.E.B., P.C. Zalm, P. Van der Sluis, D.J. Gravensteijn, and W.B. de Boer (1994). "Diffusion in strained Si(Ge)". Physical Review Letters. 72(16): p. 2585-2588.

Embury, J.D., A. Deschamps, and Y. Brechet, (2003). "The interaction of plasticity and diffusion controlled precipitation reactions". Scripta Materialia,. ??(10 SPEC.): p. 927-932.

Ernst, S.C., W.A. Baeslack, III, and J.C. Lippold (1989). "Weldability of high-strength low- expansion superalloys". Welding Journal (Miami, Fla), 68(10): p. 418s-430s.

Handwerker, C.A., J.W. Cahn, D.N. Yoon and J.E. Blendell. (1985). "The effect of coherency strain on alloy formation: migration of liquid films. in Diffusion in Solids:Recent Development". The Metallurgical Society, Warrendale, P.A., p.275.

Nakkalil, R., N.L. Richards, and M.C. Chaturvedi(1993). "Influence of solidification mode on heat affected zone microfissuring in a nickel-iron base superalloy. Acta metallurgica et materialia,. 41(12): p. 3381-3392.

Ojo, O.A., N.L. Richards, and M.C. Chaturvedi, (2004). "Liquid film migration of constitutionally liquated gamma ' in weld heat affected zone" (HAZ) of Inconel 738LC superalloy". Scripta Materialia,. 51(2): p. 141-146.

Ojo, O.A., N.L. Richards, and M.C. Chaturvedi, (2006)."Study of the fusion zone and heat affected zone microstructures in tungsten inert gas-welded INCONEL" 738LC superalloy. Metallurgical and Materials Transactions A-Physical Metallurgy and Materials Science, 37A (2): p. 421-433.

Ola, O.T., O.A. Ojo, P. Wanjara, and M.C. Chaturvedi, (2010). "Enhanced resistance to weld cracking by strain-induced rapid solidification during linear friction welding". Philosophical Magazine Letters, 91(2): p. 140-149.

Oluwasegun. K.M, O. E. Olorunniwo, And O.O.Oluwole, (2010a,)."The Contribution of Eutectic $\gamma$- $\gamma'$ Liquid Film to the TMAZ Microfissuring". In Inertia Friction Welded PM RR1000 Superalloy Journal of the Nigerian Institute of Mechanical Engineers, 2, (1): p.19-30.

Oluwasegun ,S.A.Ibitoye and O.O.Oluwole, TMAZ Microcracking in Inertia Friction Welding of PM RR1000 Superalloy: Concomitant Effect of Constitutional Liquating Particles. Journal of Engineering Research, 2010b, 15 (2): p.64-72

Owczarski, W.A., D.S. Duvall, and C.P. Sullivan, (1966). Model for heat-affected zone cracking in nickel-base superalloys. Welding Journal, 45(4): p. 145-155.

Pepe, J.J. and W.F. Savage, (1967). Effects of constitutional liquation in 18-ni maraging steel weldments. Welding Journal, 46(9): p. S411-422.

Radhakrishnan, B. and R.G. Thompson, (1990). "Liquid-film migration (lfm) in the weld heat affected zone (HAZ) of a Ni-base superalloy. Scripta Metallurgica Et Materialia,.24(3): p. 537-542.

Radhakrishnan, B. and R.G. Thompson, Phase diagram approach to study liquation cracking in alloy 718. Metallurgical transactions. A, Physical metallurgy and materials science, 1991. 22 A(4): p. 887-902.

Radhakrishnan, B. and R.G. Thompson, (1993). "The effect of weld heat-zone (HAZ) liquation kinetics on the hot cracking susceptibility of alloy-718". Metallurgical Transactions a-Physical Metallurgy and Materials Science, 24(6): p. 1409-1422.

Reiso, O., N. Ryum, and J. Strid, (1993). "Melting of secondary-phase particles in Al-Mg-Si Alloys.Metallurgical". Transactions A-Physical Metallurgy and Materials Science, 24(12): p. 2629-2641.

Romig Jr, A.D., J.C. Lippold, and M.J. Cieslak, Analytical electron microscope investigation of the phase transformations in a simulated heat-affected zone in alloy 800. Metallurgical transactions. A, Physical metallurgy and materials science, 1988. 19 A (1): p. 35-50.

Shahriari, D., M.H. Sadeghi, A. Akbarzadeh and M.Cherraghzadeh, (2009). "The influence of heat treatment and hot deformation conditions on gamma' precipitate dissolution of Nimonic 115 superalloy". International Journal of Advanced Manufacturing Technology, .45(9-10): p. 841-850.

Thompson, R.G., B. Radhakrishnan, and D.E. Mayo, (1988). "Grain-boundary chemistry contributions to intergranular hot cracking". Journal De Physique, 49(C-5): p. 471-479

Wang L., M. Preuss, P.J. Withers, G. Baxter, and P. Wilson, (2005). "Energy-input-based Finite element process modeling of inertia welding". Metallurgical and Materials Transactions B: Process Metallurgy and Materials Processing Science, 36(4): p. 513-523.